Dalton Transactions

ROYAL SOCIETY OF CHEMISTRY

PAPER

View Article Online
View Journal | View Issue

Cite this: *Dalton Trans.*, 2024, **53**, 11500

Putative reaction mechanism of nitrogenase with a half-dissociated S2B ligand†

Hao Jiang and Ulf Ryde *

We have studied whether dissociation of the S2B sulfide ligand from one of its two coordinating Fe ions may affect the later parts of the reaction mechanism of nitrogenase. Such dissociation has been shown to be favourable for the E_2–E_4 states in the reaction mechanism, but previous studies have assumed that S2B either remains bridging or has fully dissociated from the active-site FeMo cluster. We employ combined quantum mechanical and molecular mechanical (QM/MM) calculations with two density-functional theory methods, r^{2}SCAN and TPSSh. To make dissociation of S2B possible, we have added a proton to this group throughout the reaction. We study the reaction starting from the E_4 state with N_2H_2 bound to the cluster. Our results indicate that half-dissociation of S2B is unfavourable in most steps of the reaction mechanism. We observe favourable half-dissociation of S2B only when NH or NH_2 is bound to the cluster, bridging Fe2 and Fe6. However, the former state is most likely not involved in the reaction mechanism and the latter state is only an intermittent intermediate of the E_7 state. Therefore, half-dissociation of S2B seems to play only a minor role in the later parts of the reaction mechanism of nitrogenase. Our suggested mechanism with a protonated S2B is alternating (the two N atoms of the substrate is protonated in an alternating manner) and the substrate prefers to bind to Fe2, in contrast to the preferred binding to Fe6 observed when S2B is unprotonated and bridging Fe2 and Fe6.

Received 29th March 2024,
Accepted 15th June 2024

DOI: 10.1039/d4dt00937a

rsc.li/dalton

Introduction

Nitrogenase (EC 1.18/19.6.1) is the only enzyme that can cleave the triple bond in N_2, by converting it to ammonia.[1–4] Nitrogenase is produced by a few groups of bacteria but several higher plants live in symbiosis with such bacteria, *e.g.* legumes, rice and alder. Crystallographic studies have shown that the most common and active form of nitrogenase is a homodimer of heterodimers.[5–9] It contains two unusual iron–sulfur clusters, the P-cluster ($Fe_8S_7Cys_6$), which is used for electron transfer, and the FeMo cluster, which is the catalytic centre. The latter consists of a $MoFe_8S_9C$(homocitrate) cluster, which is connected to the protein by one His ligand to Mo and a Cys ligand to a Fe ion at the other end of the cluster (*cf.* Fig. 1a). There also exist alternative isoenzymes in which the Mo ion is replaced by V or Fe, but they have a lower activity.[10] During catalysis, electrons are delivered to nitrogenase by the Fe protein, which contains a Fe_4S_4 cluster.[3,4]

Nitrogenase catalyses the reaction[3,4]

$$N_2 + 8e^- + 8H^+ + 16ATP \rightarrow 2NH_3 + H_2 + 16ADP + 16P_i \quad (1)$$

Thus, eight electrons and protons are needed to form two molecules of NH_3 from N_2. Consequently, the reaction mechanism is typically described by nine states, E_0–E_8, differing in the number of added electrons and protons.[11] Despite intensive biochemical, kinetic, spectroscopic and computational investigations,[1–9,12,13] many details of the nitrogenase reaction mechanism are still controversial, partly because of technical problems to isolate pure samples of the various reaction intermediates E_n. It is known that N_2 binds mainly to the E_4 state and that N_2 binding is coupled to the compulsory formation of H_2, in a reductive elimination reaction.[14–18] E_4 has been shown to contain two hydride ions bridging two pairs of Fe ions,[15,16,18] but the detailed structure of the E_4 state is highly controversial.[19–28]

The later part of the reaction mechanism, *i.e.* after N_2 binding has also been much discussed.[3] In particular, it has been debated whether nitrogenase follows a distal or an alternating mechanism, *i.e.* whether the protons are first added to one N atom, so that NH_3 dissociates already in the E_5 state, before the second N atom is protonated, or whether protons are added alternatively to the two N atoms, so that HNNH and H_2NNH_2 are intermediates and the first NH_3 molecule does

Department of Computational Chemistry, Lund University, Chemical Centre, P. O. Box 124, SE-221 00 Lund, Sweden. E-mail: Ulf.Ryde@compchem.lu.se; Tel: +46-46 2224502

† Electronic supplementary information (ESI) available. See DOI: https://doi.org/10.1039/d4dt00937a

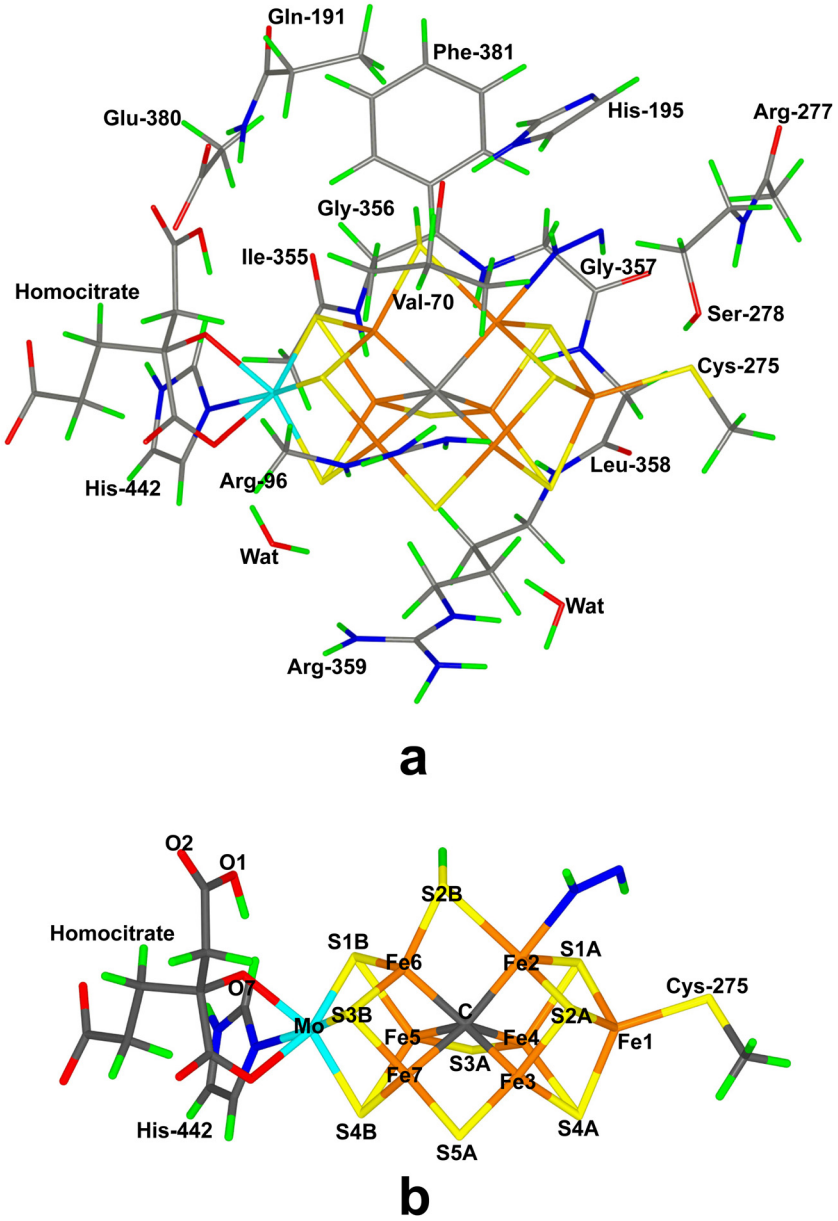

Fig. 1 The FeMo cluster in nitrogenase (*trans*(2;1A)-S2B(26;3) structure). (a) Illustrates the QM system used in all calculations, as well as the names of the nearby residues, (b) shows only the FeMo cluster with atom names indicated.

not dissociate until the E_7 state. A distal mechanism is supported by inorganic nitrogenase model complexes,[29–33] but also by some computational and crystallographic studies of nitrogenase.[25,34] An alternating mechanism is supported by the fact that H_2NNH_2 is a substrate of nitrogenase and can also be released from the enzyme by acid or base treatment during turnover.[1,3,35,36] It has also been shown that N_2, N_2H_2, CH_3N_2H and N_2H_4 all react *via* a common intermediate.[37] Several computational studies have suggested reaction mechanisms that are alternating, at least during the end of the reaction (*i.e.* involving H_2NNH_2 as an intermediate).[13,38,39]

Our group has presented several studies of the later part of the nitrogenase reaction mechanism. We have performed an exhaustive search of possible binding sites and binding modes of N_2H_2 to the FeMo cluster in the E_4 state.[40] The study showed that the most favourable binding sites were Fe2 and Fe6 (atom numbers are shown in Fig. 1b). *trans*-HNNH bound to Fe2 was most stable, but structures with the same molecule bound to Fe6, *cis*-HNNH bound to Fe2, or $HNNH_2$ bound to Fe6 (with the additional proton abstracted from homocitrate) were all competitive within 12 kJ mol^{-1}. With a somewhat larger quantum-mechanical (QM) model, including also Val-70 and Phe-381, which may restrict the binding of the substrate, the preferences change somewhat in favour of *trans*-HNNH or $HNNH_2$ binding to Fe6.[39] That study also considered the complete reaction mechanism and suggested an alternating

mechanism and that the homocitrate ligand may provide a proton buffer that may stabilise intermediates like H_2NNH_2 and NH_3 already at the E_5 and E_7 states, respectively. Based on suggestions from crystal structures of inhibited nitrogenase, we also investigated the corresponding reactions when S2B has dissociated from the FeMo cluster, providing a natural binding site for the substrate.[38] The results suggested that N_2H_2 binds as NNH_2 bridging Fe2 and Fe6 (*i.e.* an intermediate connected to a distal mechanism), but that the mechanism the becomes alternating, with H_2NNH_2 bound at the E_6 state and NH_3 formation in the E_7 state. Both mechanism seemed to be equally feasible, but a study of proton-transfer reactions in the cluster indicated that the proton transfer to the substrate is easier if S2B remains bound.[41]

Several recent studies have suggested that S2B may dissociate only from one of the two Fe ions, forming unhooked or half-dissociated structures.[21,42–44] In fact, such structures seem to be among the most likely candidates for the E_2–E_4 states of Mo-nitrogenase.[22,44,45] The question then naturally arises whether such structures are competitive also for the later part of the nitrogenase reaction, *i.e.* after binding of N_2. The aim of the present study is to investigate this possibility using combined QM and molecular mechanics (QM/MM) calculations.

Methods

The protein

The calculations were based on the 1.0 Å crystal structure of Mo nitrogenase from *Azotobacter vinelandii* (PDB code 3U7Q).[5] The setup of the protein is identical to that of our previous studies.[20,22,46–48] The entire heterotetramer was included in the calculations and the QM calculations were concentrated on the FeMo clusters in the C subunit because there is a buried imidazole molecule rather close to the active site (~11 Å) in the A subunit. The two P clusters and the FeMo cluster in subunit A were modelled by molecular mechanics (MM) in the fully reduced and resting states, respectively, using a QM charge model.[47] The protonation states of all residues were the same as before,[47] and the homocitrate ligand was modelled in the singly protonated state with a proton shared between the hydroxyl group (O7 that coordinates to Mo) and the O1 carboxylate atom.[47,49] The protein was solvated in a sphere with a radius of 65 Å around the geometrical centre of the protein. Cl^- and Na^+ ions were added to yield an ionic strength of 0.2 M.[50] The final system contained 133 915 atoms. For the protein, we used the Amber ff14SB force field[51] and water molecules were described by the TIP3P model.[52] The metal sites were treated by a non-bonded model[53] and charges were obtained with the restrained electrostatic potential method.[54]

In the QM calculations, the FeMo cluster was modelled by $MoFe_7S_9C$(homocitrate)(CH_3S)(imidazole), where the two last groups are models of Cys-275 and His-442. In addition, all groups that form hydrogen bonds to the FeMo cluster were also included, *viz*. Arg-96, Gln-191 and His-195 (sidechains), Ser-278 and Arg-359 (both backbone and sidechain, including the CA and C and O atoms from Arg-277), Gly-356, Gly-357 and Leu-358 (backbone, including the CA and C and O atoms from Ile-355), as well as two water molecules. Finally, the sidechain of Glu-380 was included because it forms hydrogen bonds to Gln191 and His-442, as well as the sidechains of Val-70 and Phe-381 because they are close to S2B, Fe2 and Fe6, *i.e.* the expected reactive site. The QM system contained 192–197 atoms depending on the E_n state and the bound substrate. It is shown in Fig. 1a. The net charge of QM region was $-3e$.

QM calculations

All QM calculations were performed with the Turbomole software (versions 7.5 and 7.6).[55] All structures were studied with the r^{2}SCAN[56] density functional theory (DFT) method. To investigate the functional dependence, most structures were also studied with the TPSSh[57] functional. r^{2}SCAN is a *meta* generalised gradient approximation functional, whereas TPSSh is a hybrid functional with 10% Hartree–Fock exchange. Both functionals have been shown to give accurate structures of nitrogenase models.[58] All calculations involved the def2-SV(P) basis set.[59] The calculations were sped up by expanding the Coulomb interactions in an auxiliary basis set, the resolution-of-identity (RI) approximation.[60,61] Empirical dispersion corrections were included with the DFT-D4 approach,[62] as implemented in Turbomole.

In this investigation we study the later part of the reaction mechanism of nitrogenase, starting after the binding and protonation of the substrate to N_2H_2 in the E_4 state. Like in our previous two studies,[38,39] we do this to avoid the problem that the nature of the E_4 state is highly controversial, with a very large number of possible locations of the added four H atoms (protons or hydride ions), and extremely large discrepancy in the prediction of various DFT methods.[13,20–23,46] The current consensus is that N_2 binds to the FeMo cluster together with reductive elimination of H_2.[4] The remaining two protons are then used to protonate N_2 to N_2H_2. As a consequence, the N_2H_2-bound E_4 state is in the same formal oxidation state as the resting E_0 state, *viz*. the $Mo^{III}Fe_3^{II}Fe_4^{III}$ oxidation state.[49,63,64]

The aim of the present study is to investigate whether dissociation of S2B from either Fe2 or Fe6 may facilitate the conversion of N_2H_2 to two NH_3 molecules. Previous studies have shown that such half-dissociation of S2B is energetically favourable only if S2B is protonated.[21,43,44] Therefore, we added an extra proton to S2B in all the current models. Consequently, the charge of the models is one step less negative than previously studied models.

The electronic structure in all QM calculations was obtained with the broken-symmetry (BS) approach:[65] Each of the seven Fe ions was modelled in the high-spin state, with either a surplus of α (four Fe ions) or β (three Fe ions) spin. Such a state can be selected in 35 different ways.[65,66] The various BS states were obtained either by swapping the coordinates of the Fe ions[67] or with the fragment approach by Szilagyi and Winslow.[68] The BS states are named by listing the numbers of the three Fe ions with minority spin, *e.g.* BS-235. At each E_n-level, we first optimised all possible structures with

one BS state (typically BS-235 or BS-147). For the most stable structure, a full investigation of all 35 BS was performed and if this was a different state, the best structures are reoptimised with that state. A similar procedure was performed with the spin state, which is also unknown for these intermediates.

QM/MM calculations

QM/MM calculations were performed with the ComQum software.[69,70] In this approach, the protein and solvent are split into two subsystems: system 1 (the QM region) was relaxed by QM methods. System 2 was kept fixed at the original coordinates (equilibrated crystal structure), to avoid the risk that different calculations end up in different local minima.

In the QM calculations, system 1 was represented by a wavefunction, whereas all the other atoms were represented by an array of partial point charges, one for each atom, taken from the MM setup (electrostatic embedding). Thereby, the polarisation of the QM system by the surroundings is included in a self-consistent manner. When there is a bond between systems 1 and 2 (a junction), the hydrogen link-atom approach was employed: the QM system was capped with hydrogen atoms, the positions of which are linearly related to the corresponding carbon atoms (carbon link atoms, CL) in the full system.[69,71] All atoms were included in the point-charge model, except the CL atoms.[72] ComQum employs a subtractive scheme with van der Waals link-atom corrections.[73] No cut-off is used for the QM and QM–MM interactions. The geometry optimisations were continued until the energy change between two iterations was less than 2.6 J mol^{-1} (10^{-6} a.u.) and the maximum norm of the Cartesian gradients was below 10^{-3} a.u.

In most structures where S2B binds to both Fe2 and Fe6, one Fe–S distance is ~2.3 Å and the other 0.1–0.3 Å longer. Thereby, S2B is in between the two Fe ions and both Fe–Fe–S2B angles are less than 90°. When S2B dissociates from one of the Fe ions, the substrate typically bridges Fe2 and Fe6 (with one or two N atoms) and one Fe–S2B distance increases to >3.4 Å and one Fe–Fe–S2B angle is larger than 90°. However, in some cases, the substrate binds only to one Fe ion and S2B to the other ion (often, but not always, receiving a hydrogen bond from the substrate). In those cases, it is less obvious whether S2B has dissociated or not. We used a cutoff of Fe–S2B > 2.9 Å to define a dissociated structure (no structure has a Fe–S2B bond length between 2.81 and 3.04 Å; likewise, there is a gap between 0.52 and 0.86 Å for the absolute difference between the two Fe–S2B distances). Mayer bond orders[74] (calculated with the Multiwfn package[75]) for the Fe–S interactions are correlated to the Fe–S distances (correlation coefficient −0.87) and show similar trends; a cutoff at 0.2 can be used to define bonds.

Results and discussion

In this investigation, we have studied possible paths for the second half of the mechanism of nitrogenase, allowing the S2B ligand to dissociate from one Fe ion. The results are compared to our previous studies where S2B was either binding to both Fe2 and Fe6,[39] or was completely dissociated.[38] As in the previous studies, we start from a E_4 state, where H_2 has dissociated, N_2 is bound and is protonated to N_2H_2. This is done to avoid the severe problems that different DFT method give widely different predictions regarding the most stable protonation states of E_4 and the strength of the binding of N_2.[22,46]

For each new E_n state, we add one electron and a proton to the FeMo cluster. The electrons are provided by the Fe protein *via* the P-cluster.[2,3] Protons come ultimately from water solvent and two possible proton channels have been suggested, ending either at His-195 or at a water molecule close to S3B, S4B and S5A.[76–79] It has suggested that His-195 can only provide a single proton, because rotation of the imidazole group is restricted in the protein.[76,80] Several groups have studied proton transfers within the FeMo cluster and have shown that the individual steps in general are facile,[76,78,81] although sometimes certain protonation states may act as thermodynamic sinks making the net barriers somewhat high.[41] However, Siegbahn has suggested that the barriers are strongly lowered by the employment of surrounding water molecules.[28,82] Therefore, we have not explicitly studied proton transfers within the FeMo cluster in this study. Instead we concentrate on determining the thermodynamically most stable structures at each E_n level and the cleavage of the N–N bond. We discuss the various E_n states in separate sections.

E_4 state

We started with the E_4 state with N_2H_2 bound. We tested four different isomers of N_2H_2, *viz.* NNH_2, *cis*-HNNH, *trans*-HNNH and $HNNH_2$ (in the latter case, the third proton was taken from homocitrate, which is nearby when the ligand binds to Fe6). We studied binding of N_2H_2 only to Fe2 and Fe6, because these two Fe ions have been pointed out by experimental studies[3,83,84] and it has also been shown to be the preferred binding sites by a systematic DFT search.[40] We studied both end-on and side-on binding, to one Fe ion as well as to both Fe ions. If relevant, we allowed the non-coordinating N atom or the protons to point in different directions. We use the following nomenclature: the four isomers are called NNH_2, *cis*, *trans* or $HNNH_2$, respectively, which is followed by the binding site in brackets and indicating only the number of the Fe atom. 2 and 6 means that it binds to only Fe2 or Fe6, whereas 26 means that it bridges Fe2 and Fe6. Two numbers with a comma between means that both N atoms bind to Fe, *e.g.* (26,2), indicating that one N atom bridges Fe2 and Fe6, whereas the other binds only to Fe2. A number or an atom after a semicolon indicates the direction of the non-coordinating atoms, where 3 and 5 indicate S3A and S5A, respectively.

In addition, we considered structures with the S2B ligand bridging Fe2 and Fe6 or binding only to one of the two Fe ions. In variance to the previous study,[39] we assumed that S2B is singly protonated, allowing it to dissociate from either Fe2 or Fe6. When it still bound to both ions, we tried to force it to dissociate from one of the Fe ions. Moreover, we also studied cases where the proton on S2B pointed in different directions,

typically towards S3A or S5A. The nomenclature is S2B with the coordinating Fe ions in brackets (2, 6, or 26) and with the direction indicated after a semicolon with numbers 3 or 5, or an atom.

We tested 61 different structures and managed to obtain 53 of them. They are listed in Table 1. It can be seen that the most stable structure is *trans*(2;1A)-S2B(26;3), *i.e.* with *trans*-HNNH binding to Fe2 with the non-bonding NH group pointing towards S1A (with a S–H hydrogen-bonding distance of 2.2 Å), and with S2B coordinating to both Fe2 and Fe6, with the proton pointing towards S3A. It is most stable in the quartet BS-235 state and it is shown in Fig. 2. Cleaving the Fe2–S2B bond is strongly unfavourable, so the best structure does not have any half-dissociated S2B group. Moving the proton on S2B to the opposite side, *trans*(2;1A)-S2B(26;5) (also in Fig. 2), changes the energy by only 3–4 kJ mol^{-1}. The corresponding structures with HNNH binding instead to Fe6 are only 6 kJ mol^{-1} less stable with the r^{2}SCAN functional, but 12–13 kJ mol^{-1} with TPSSh (*trans*(6;3B)-S2B(26;3) and *trans*(6;3B)-S2B(26;5) in Fig. 2). In this case, the non-coordinat-

Table 1 Relative energies (kJ mol^{-1}) of the various structures optimised for the E_4 state. All structures are in the quartet BS-235 state unless otherwise noted

Structure	r^{2}SCAN	TPSSh
$HNNH_2$(6;HCA)-S2B(26;3)	45	39
$HNNH_2$(6;HCA)-S2B(26;5)	38	57
NNH_2(26)-S2B(2;Fe1)	21	31
NNH_2(26)-S2B(2;5)	34	39
NNH_2(26)-S2B(6;3B)	18	24
NNH_2(26)-S2B(6;1B)	18	40
NNH_2(2;1A)-S2B(26;3)	15	6
NNH_2(2;1A)-S2B(26;5)	25	33
NNH_2(2;2A)-S2B(6;3)	60	57
NNH_2(2;2A)-S2B(26;5)	76	71
NNH_2(6;1B)-S2B(2;Fe1)	80	96
NNH_2(6;2B)-S2B(2;4A)	91	
NNH_2(6;HCA)-S2B(26,3)	56	57
NNH_2(6;3)-S2B(26;5)	66	74
cis(26;3)-S2B(2;Fe1)	114	111
cis(26;3)-S2B(2;5)	129	139
cis(26,2;3)-S2B(6;N)	41	45
cis(26,2;5)-S2B(6;Mo)	34[a]	52
cis(26,2;5)-S2B(6;3)	27[a]	45
cis(26,6;3)-S2B(2;Fe1)	88	90
cis(26,6;3)-S2B(2;5)	102	104
cis(26,6;5)-S2B(2;Fe1)	71	73
cis(26,6;5)-S2B(2;3)	90	95
cis(26,6;5)-S2B(2;5)	78	81
cis(2,6)-S2B(2;Fe1)	103[b]	108
cis(2,6)-S2B(2;5)	84[a]	109
cis(2,6)-S2B(6;Mo)	92[a]	112
cis(2,2)-S2B(6;3B)	81	99
cis(2,2)-S2B(6;3)	76	94
cis(2;1A)-S2B(26;3)	9	11
cis(2;1A)-S2B(26;5)	14	16
cis(2;2A)-S2B(26;3)	61	64
cis(2;2A)-S2B(26;5)	60	52
cis(6,6;5)-S2B(2;2A)	130	
cis(6,6)-S2B(2;Fe1)	130	
cis(6;1B)-S2B(26;3)	29	34
cis(6;1B)-S2B(26;5)	30	37
cis(6;3B)-S2B(26;3)	40	47
cis(6;3B)-S2B(26;5)	39	46
trans(26;5)-S2B(2;Cys)	83[b]	86
trans(26;5)-S2B(2;N)	94	99
trans(26,2;5)-S2B(6;3B)	41	35
trans(26,2;5)-S2B(6;N)	33	28
trans(26;3)-S2B(2;Cys)	47	57
trans(2;1A)-S2B(26;3)	0	0
trans(2;1A)-S2B(26;5)	3	4
trans(2;2A)-S2B(6;3)	34	39
trans(2;2A)-S2B(26;5)	41	44
trans(6;1B)-S2B(26;3)	17	22
trans(6;1B)-S2B(26;5)	23	27
trans(6;3B)-S2B(26;3)	6	12
trans(6;3B)-S2B(26;5)	6	13

[a] Quartet BS-147 state. [b] Doublet BS-147 state.

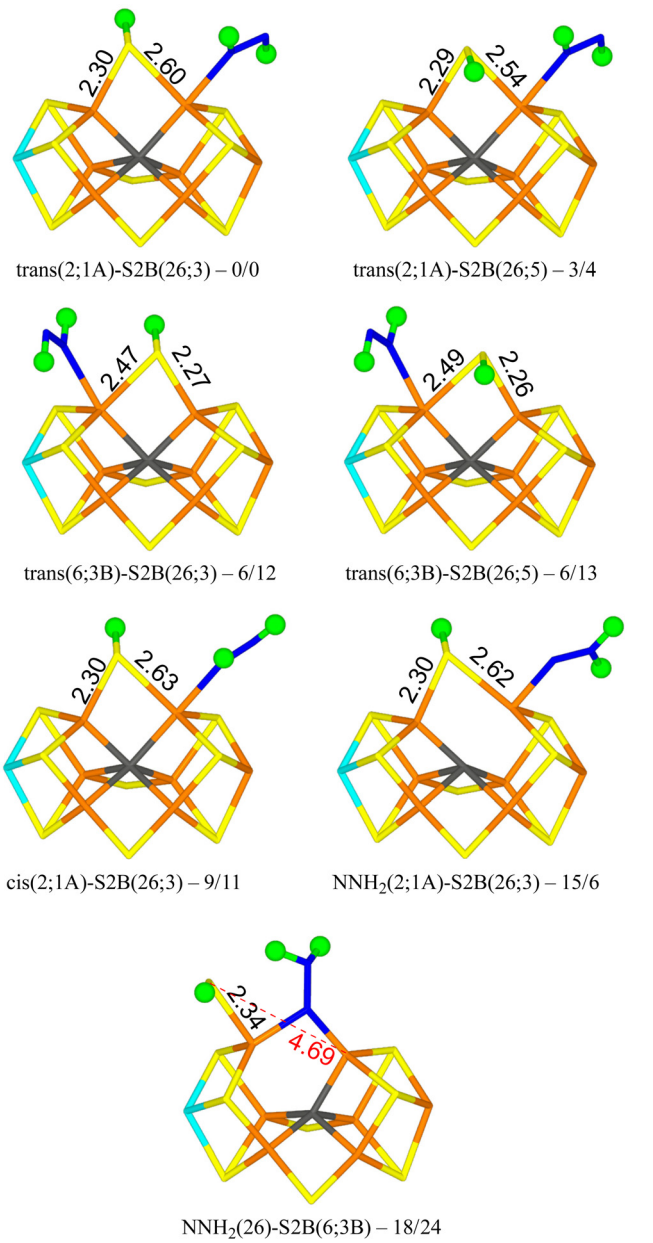

Fig. 2 The best E_4 structures with relative energies in kJ mol^{-1} indicated (r^{2}SCAN/TPSSh).

ing N atom of HNNH forms a hydrogen bond to S3B (2.6 Å). On the other hand, structures with HNNH pointing in the opposite direction are appreciably less stable, by 34–44 kJ mol^{-1} when HNNH binds to Fe2 and 17–27 kJ mol^{-1} when it binds to Fe6. The non-coordinating N atom still forms hydrogen bonds to the cluster (2.4 Å to S2A or 2.5 Å to S1B), but Val-70 and Ser-278 are strongly restricting its movement.

Structures with *cis*-HNNH binding to Fe2 (*e.g. cis*(2;1A)-S2B (26;3) in Fig. 2) are also competitive, 9–16 kJ mol^{-1} less stable than the best one, and still with S2B binding to both Fe2 and Fe6. The non-bonding N atom is still pointing towards S1A, but no hydrogen bond can form for the *cis*-isomer of the ligand. The opposite orientation of HNNH is much less stable, owing to steric interactions with Val-70 and Ser-278. Likewise, *cis*-HNNH binding to Fe6 is quite unfavourable, 29–46 kJ mol^{-1} less stable than the best structure.

A structure with NNH_2 binding to Fe2 is also competitive, NNH_2(2;1A)-S2B(26,3) in Fig. 2, especially with TPSSh, being 6–15 kJ mol^{-1} less stable than the best structure. The non-bonding N atom forms a hydrogen bond to S1A (2.3 Å) and S2B binds to both Fe2 and Fe6. Structures with the substrate pointing instead towards S2A (2.3 Å hydrogen-bonding distance) is ~50 kJ mol^{-1} less stable.

The best structure with a half-dissociated S2B ligand is NNH_2(26)-S2B(6;3B) in Fig. 2 with r^2SCAN, *i.e.* with NNH_2 bridging Fe2 and Fe6, and with one of the H atoms forming a hydrogen bond to S2B (2.14 Å H–S distance). S2B is dissociated from Fe2, but binds to Fe6. Its proton is pointing towards S3B (2.9 Å distance). The structure with the proton on S2B pointing in the opposite direction (towards S3B) is essentially degenerate, 18 kJ mol^{-1} less stable than the best *trans*(2;1A)-S2B(26;3) structure. With TPSSh, the latter structure is most stable by 16 kJ mol^{-1}, 24 kJ mol^{-1} less stable than the best structure.

These results are quite similar to what has been observed in our previous studies: *trans*-HNNH binding to either Fe2 and Fe6 is nearly degenerate when S2B remains bound and bridging NNH_2 most stable without S2B.[38–40] The largest difference is that the $HNNH_2$ structures are not competitive, being 38–57 kJ mol^{-1} less stable than the best structures. The reason may be the extra proton on S2B, which makes the hydrogen bond between the substrate and S2B less favourable (2.42 Å, compared to 2.24 Å in our previous study[40]) and also orients the substrate so that the hydrogen bond to homocitrate is worse (1.97 Å, compared to 1.69 Å (ref. 40)). However, the most important conclusion is that there is no advantage of S2B dissociation in the N_2H_2-bond E_4 state.

E_5 state

Next, we added one proton and one electron to consider the E_5 state. We studied four variants of the substrate, $HNNH_2$, NNH_3, H_2NNH_2 (hydrazine) and $HNNH_3$. In the latter two cases, the substrate has abstracted a proton from homocitrate. As for E_4, we studied both end-on and side-on binding, to Fe2, Fe6 or both. Likewise, we considered structures with S2B bound to only Fe2 or Fe6, or to both. The structures are named as in the previous section and the results are listed in Table 2.

Table 2 Relative energies (kJ mol^{-1}) of the various structures optimised for the E_5 state. All structures are in the quintet BS-235 state unless otherwise noted

Structure	r^2SCAN	TPSSh
H_2NNH_2(6;1B)-S2B(26;3)	11	29
H_2NNH_2(6;1B)-S2B(26;5)	11	24
H_2NNH_2(6;2B)-S2B(26;3)	9	20
H_2NNH_2(6;2B)-S2B(26;5)	14	32
H_2NNH(26,6)-S2B(2;Cys)	90	82
H_2NNH(26,6)-S2B(2;2A)	96	91
H_2NNH(2,6)-S2B(6;3B)	113	120
H_2NNH(2,6)-S2B(6;1B)	117	
H_2NNH(2;2B)-S2B(6;3B)	79	93
H_2NNH(2,2)-S2B(6;1B)	40	51
$HNNH_2$(6,2)-S2B(2;Cys)	109	112
$HNNH_2$(6,2)-S2B(2;N)	121	114
$HNNH_2$(2,2)-S2B(6;3B)	47	42
$HNNH_2$(2,2)-S2B(6;1B)	37	49
$HNNH_2$(2;2A)-S2B(6;3B)	36	43
$HNNH_2$(2;2A)-S2B(6;1B)	28	35
$HNNH_2$(2;Cys)-S2B(6;1B)	9[a]	15[b]
$HNNH_2$(2;1A)-S2B(26;3)	0	0
$HNNH_2$(2;1A)-S2B(26;5)	7	8
$HNNH_2$(2;2A)-S2B(6;1B)	45	
$HNNH_2$(2;2A)-S2B(26;5)	67	68
$HNNH_2$(6,6)-S2B(2;Cys)	139	146
$HNNH_2$(6;2B)-S2B(26;3)	47	53
$HNNH_2$(6;2B)-S2B(26;5)	32	55
$HNNH_3$(6;1B)-S2B(26;3)	82	93
$HNNH_3$(6;1B)-S2B(26;5)	76	88
$HNNH_3$(6;3B)-S2B(26;3)	80	80
$HNNH_3$(6;3B)-S2B(26;5)	67	75
NNH_3(26)-S2B(2;1A)	140	139
NNH_3(26)-S2B(2;2A)	131	134
NNH_3(26)-S2B(6;3B)	59	79
NNH_3(26)-S2B(6;1B)	53	76
NNH_3(2;1A)-S2B(26;3)	137	131
NNH_3(2)-S2B(26;5)	143	137
NNH_3(6;2B)-S2B(2;2A)	218	243
NNH_3(6;1B)-S2B(26;3)	197	214
NNH_3(6;1B)-S2B(26;5)	186	197
NNH_3(6;3B)-S2B(26;3)	180	190
NNH_3(6;3B)-S2B(26;5)	185	191

[a] BS-247 state. [b] BS-147 state.

We tried to optimise 45 structures and 39 of them were obtained. The best ($HNNH_2$(2;1A)-S2B(26;3)) has $HNNH_2$ bound to Fe2, with the non-coordinating NH_2 group pointing towards S1A, forming a hydrogen bond with a H–S1A distance of 2.22 Å. The structure is most stable in the quintet BS-235 state and is shown in Fig. 3. The other H atom of the NH_2 group points towards the backbone NH group of Ser-278 in a perpendicular manner (2.18 Å H–N distance). S2B binds both Fe2 and Fe6, with the proton on the S3A side. Dissociating S2B from Fe2 is strongly unfavourable. Moving the proton to the other side gives a structure that is 7–8 kJ mol^{-1} less stable ($HNNH_2$(2;1A)-S2B(26;5) in Fig. 3). On the other hand, rotating the substrate around the Fe2–N bond so that the NH_2 group instead forms a hydrogen bond to S2A (2.37 Å), gives a structure that is 45 kJ mol^{-1} less stable and S2B dissociates from Fe2. Likewise, structures with $HNNH_2$ binding to Fe6 are quite unfavourable (by 32–55 kJ mol^{-1}).

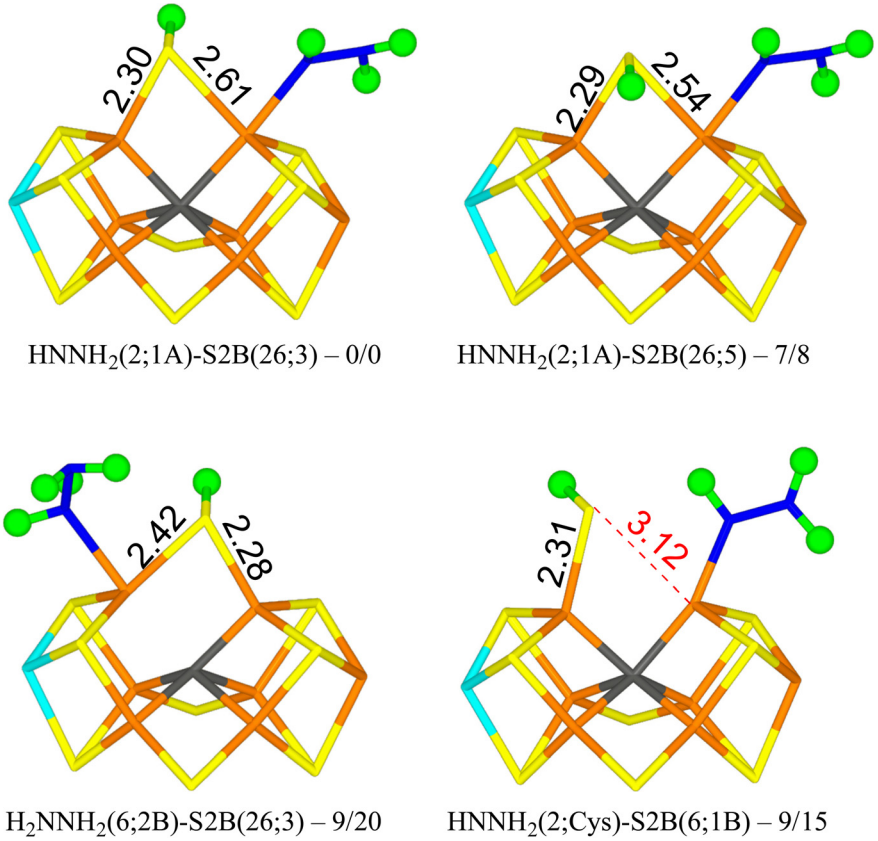

Fig. 3 The best E_5 structures with relative energies in kJ mol^{-1} indicated (r^{2}SCAN/TPSSh).

With r^{2}SCAN, structures with H_2NNH_2 bound to Fe6 are competitive, only 8–14 kJ mol^{-1} less stable than $HNNH_2$(2;1A)-S2B(26;3). The best is H_2NNH_2(6;2B)-S2B(26;3) in Fig. 3, in which one proton on the binding NH_2 group points to the alcohol oxygen of homocitrate (2.11 Å), whereas the two protons of the non-bonding NH_2 group point towards S2B (2.36 Å) and an acetate oxygen of homocitrate (3.13 Å) but with far from optimal hydrogen-bond geometries (explaining why the various conformations have similar energies). With TPSSh, these structures are 20–32 kJ mol^{-1} less stable than the best structure.

The best structure with S2B half-dissociated is $HNNH_2$(2;Cys)-S2B(6;1B) in Fig. 3, *i.e.* with $HNNH_2$ binding end-on to Fe2, the non-bonding NH_2 group forming a hydrogen bond to SG of Cys-275 (2.77 Å) and the proton of the bonding NH group pointing towards S2B (2.55 Å). S2B binds only to Fe6 with the proton pointing towards S1B. It is only 9–15 kJ mol^{-1} less stable than the best structure.

Structures with $HNNH_3$ binding to Fe6 are quite unfavourable, 67–93 kJ mol^{-1} less stable than the best structure. They all have S2B binding to both Fe2 and Fe6. Structures with NNH_3 are strongly unfavourable by 131–243 kJ mol^{-1}. The only exception are two structures with the unprotonated N atom bridging Fe2 and Fe6, S2B binding only to Fe6 and the proton on S2B pointing either two S1B or S3B. They are 53–59 (r^{2}SCAN) or 76–79 kJ mol^{-1} less stable than the best structure.

Table 3 Relative energies (kJ mol^{-1}) of the various structures optimised for the E_6 state with an intact N–N. bond. All structures are in the quartet BS-235 state unless otherwise noted

Structure	r^{2}SCAN	TPSSh
H_2NNH_2(2,6)-S2B(2;Cys)	133[a]	131
H_2NNH_2(2,6)-S2B(6;3B)	161	148
H_2NNH_2(2,6)-S2B(6;1B)	173	160
H_2NNH_2(2;1A)-S2B(6;3B)	118	107
H_2NNH_2(2;1A)-S2B(26;3)	3	−1
H_2NNH_2(2;1A)-S2B(26;5)	17	9
H_2NNH_2(2;2A)-S2B(26;3)	33	27
H_2NNH_2(2;2A)-S2B(26;5)	25	20
H_2NNH_2(6;HCA)-S2B(2;2A)	47	52
H_2NNH_2(6;1B)-S2B(26;3)	13	13
H_2NNH_2(6;1B)-S2B(26;5)	11	11
H_2NNH_2(6;3B)-S2B(26;3)	0	0
H_2NNH_2(6;3B)-S2B(26;5)	1	2
H_2NNH_3(6;3B)-S2B(26;3)	24	21
H_2NNH_3(6;3B)-S2B(26;5)	25	23
$HNNH_3$(2;1A)-S2B(26;3)	63	58
$HNNH_3$(2;1A)-S2B(26;5)	71	67
$HNNH_3$(2;2A)-S2B(26;3)	113	103
$HNNH_3$(2;2A)-S2B(26;5)	118	108
$HNNH_3$(6;1B)-S2B(26;3)	95	97
$HNNH_3$(6;1B)-S2B(26;5)	97	100
$HNNH_3$(6;3B)-S2B(26;3)	102	107
$HNNH_3$(6;3B)-S2B(26;5)	103	101
NH_3 + NH_2(6)-S2B(26,3)	85	93
NH_3 + NH(26)-S2B(6,3)	49	−10

[a] BS-147 state.

E_6 state

We next studied the E_6 state by adding another electron and proton to the E_5 state. We considered three variants of the substrate: H_2NNH_2, $HNNH_3$ or H_2NNH_3 (in the latter case with one proton abstracted from homocitrate). In total, 26 structures were tested and 24 of these were obtained. They are described in Table 3.

The best structure with r^{2}SCAN, H_2NNH_2(6;3B)-S2B(26;3) in Fig. 4, has H_2NNH_2 bound end-on to Fe2. The two H atoms of the non-coordinating NH_2 group point towards S2B and S3B with distances of 2.53 and 2.83 Å, respectively. One of the H atoms of the coordinating NH_2 group points towards the alcohol and acetate O atoms of homocitrate with distances of 2.28 and 2.27 Å, but the two O atoms are also involved in an internal hydrogen bond (1.42 Å) and a hydrogen bond to the sidechain NH_2 group of Gln-191. S2B bridges Fe2 and Fe6, and the proton points towards S3A. The structure is most stable in the quartet BS-235 state. The structure with the proton on S2B pointing in the opposite direction (H_2NNH_2(6;3B)-S2B(26;5) in Fig. 4) is only 1–2 kJ mol^{-1} less stable.

A structure with the non-bonding NH_2 group of the substrate pointing in the opposite direction (H_2NNH_2(6;1B); with the H atoms pointing towards S2B and S1B with distances of

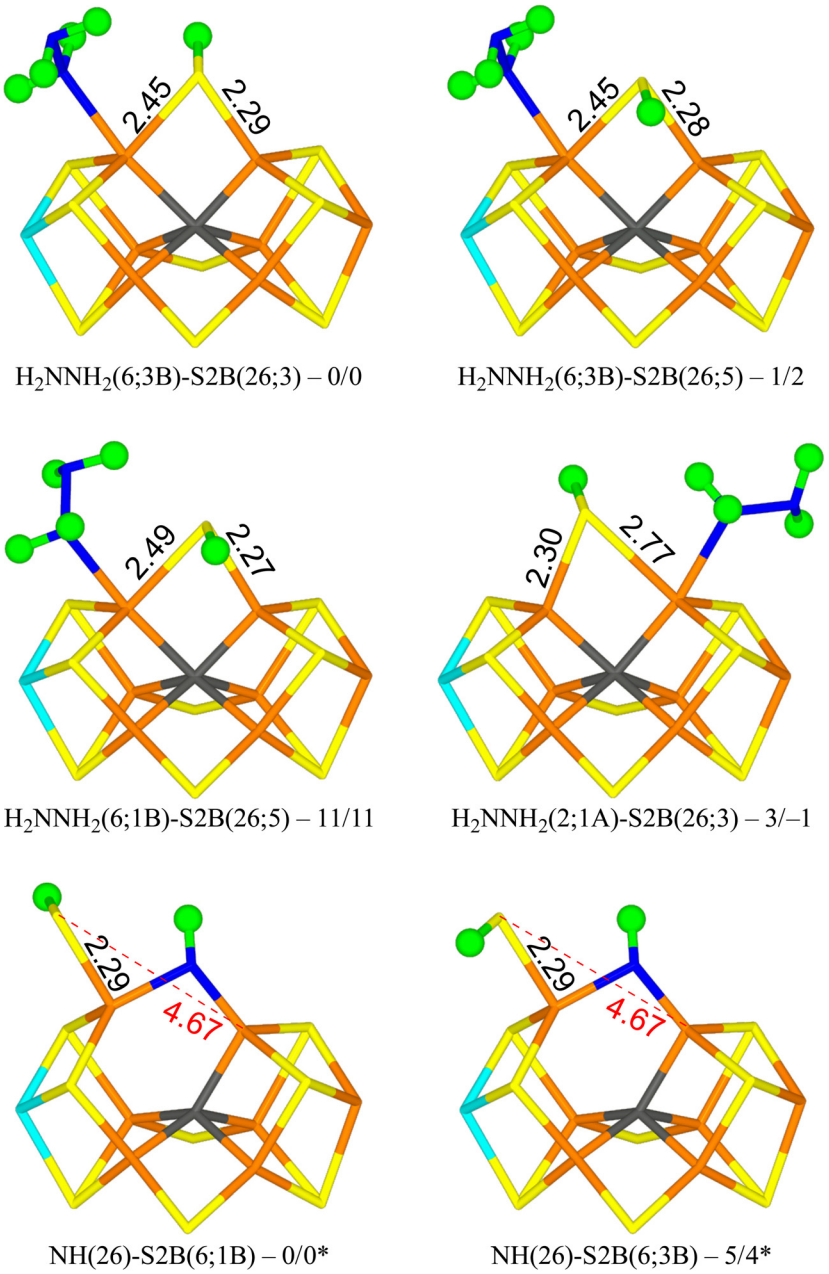

Fig. 4 The best E_6 structures with relative energies in kJ mol^{-1} indicated (r^{2}SCAN/TPSSh; * indicates a distinct reference state).

2.48 and 2.97 Å) is 11–13 kJ mol^{-1} less stable (*e.g.* H_2NNH_2(6;1B)-S2B(26;5) in Fig. 4). Still a third conformation, with the non-bonding NH_2 group pointing towards homocitrate, which leads to dissociation of S2B from Fe6 (H_2NNH_2(6;HCA)-S2B(2;2A)), is 47–52 kJ mol^{-1} less stable than the best structure and is the most stable structure with a half-dissociated S2B.

Structures with H_2NNH_2 binding to Fe2 are strongly competitive. The best is H_2NNH_2(2;1A)-S2B(26;3) in Fig. 4, *i.e.* with one H atom of the non-coordinating NH_2 group forming a hydrogen bond to S1A at a distance of 2.32 Å. Both the H atoms of the coordinating NH_2 group point towards S2B, but with poor hydrogen-bond geometries and distances of 2.61 and 3.00 Å. S2B binds to both Fe2 and Fe6, but with quite different distances of 2.77 and 2.30 Å. This structure is only 3 kJ mol^{-1} less stable than the best structure. With TPSSh, it is actually 1 kJ mol^{-1} better. In both cases, it is most stable in the quartet BS-235 state. This probably the most relevant isomer for the E_6 state, considering that the best structures of the E_4 and E_5 states had the substrate bound to Fe2. The corresponding S2B(26;3) structure is 10-14 kJ mol^{-1} less stable. Several other conformations of the substrate and the proton on S2B were also tested and they are 4–30 kJ mol^{-1} less stable. We also tested some structures with H_2NNH_2 bridging Fe2 and Fe6 and with S2B binding to only one of the Fe ions. However, they were all unfavourable by 131–173 kJ mol^{-1}.

Two structures with H_2NNH_3 bound to Fe6 were optimised. They were 21–25 kJ mol^{-1} less stable than the best one, indicating that proton transfer from homocitrate is slightly uphill.

Eight structures with $HNNH_3$ binding to either Fe2 or Fe6 were also tested, but they were all unfavourable by 58–118 kJ mol^{-1}. This shows that hydrazine is the most stable isomer of the substrate at the E_6 state. Again, structures with S2B half-dissociated seem to be of minor relevance.

We have tried to cleave the N–N bond in the two best structures (H_2NNH_2(2;1A)-S2B(26;3) and H_2NNH_2(2;1A)-S2B(26;3)). However, the reaction is quite prohibitive with barriers of 90–128 kJ mol^{-1} and the product is higher in energy than the starting structures.

For completeness, we also evaluated E_6 structures after dissociation of NH_3, *i.e.* structures with only NH bound to the FeMo cluster. Two structures with NH_2 bound to Fe6, after abstraction of the proton from homocitrate were also considered. The results are gathered in Table 4.

The most stable state has NH bridging the Fe2 and Fe6 ions, and S2B binding only to Fe6 with the proton pointing towards S1B (NH(26)-S2B(6;1B) in Fig. 4). A structure with the proton pointing instead towards S3B is only 4–5 kJ mol^{-1} less stable (NH(26)-S2B(6;3B) in Fig. 4). Structures with S2B binding only to Fe2 are 37–44 kJ mol^{-1} less stable, whereas structures with NH binding only to Fe2 or Fe6 are 120–205 kJ mol^{-1} less stable. The two structures with NH_2 binding to Fe6 are 79–91 kJ mol^{-1} less stable. Thus, structures with S2B half-dissociated are important when NH binds to the cluster. However, compared to the structures with an intact N–N bond, the HN structures are 31–46 kJ mol^{-1} less stable (adding the energy of an isolated NH_3 molecule in a water-like continuum solvent).

Table 4 Relative energies (kJ mol^{-1}) of the various structures optimised for the E_6 state with NH_3 dissociated. All structures are in the quartet BS-235 state unless otherwise noted

Structure	r^{2}SCAN	TPSSh
NH_2(6)-S2B(26;3)	86	79
NH_2(6)-S2B(26;5)	87[a]	82
NH(26)-S2B(2;Cys)	40	37
NH(26)-S2B(2;5A)	44	41
NH(26)-S2B(6;3B)	5	4
NH(26)-S2B(6;1B)	0	0
NH(2;1A)-S2B(26;3)	120	99
NH(2;1A)-S2B(26;5)	127	108
NH(2)-S2B(6;HCA)	160	136
NH(6;1B)-S2B(2;Cys)	205	201
NH(6;3A)-S2B(2;Cys)	192	189
NH(6;3A)-S2B(26;3)	130[a]	130
NH(6;3A)-S2B(26;5)	142[a]	130

[a] BS-147 state.

E_7 state

Next, we added an electron and a proton to reach state E_7. We studied first the H_2NNH_3 form of the substrate. The results are gathered in Table 5. The most stable structure has H_2NNH_3 bound end-on to Fe2 with the non-bonded NH_3 group forming a hydrogen bond to S1A (1.92 Å) and with another of the H atoms pointing transversely to the backbone N atom of Ser-278 (1.90 Å). S2B bridges Fe2 and Fe6 with the proton on the S3A side (H_2NNH_3(2;1A)-S2B(26;3) in Fig. 5). It is most stable in the triplet BS-147 state. A structure with the S2B proton on the other side is 10 kJ mol^{-1} less stable. Structures with the non-bonding NH_3 group pointing in the other direction, forming hydrogen bonds to S2A and S2B (2.13 and 2.16 Å) and with one of the NH_2 protons forming a hydrogen bond to SG of Cys-275 (2.68 Å) are 26–43 kJ mol^{-1} less stable.

Table 5 Relative energies (kJ mol^{-1}) of the various structures optimised for the E_7 state with an intact N–N. bond. All structures are in the triplet BS-147 state unless otherwise noted

Structure	r^{2}SCAN	TPSSh
H_2NNH_3(2;1A)-S2B(26;3)	173	149
H_2NNH_3(2;1A)-S2B(26;5)	183	158
H_2NNH_3(2;2A)-S2B(26;3)	199	177
H_2NNH_3(2;2A)-S2B(26;5)	214	192
H_2NNH_3(6;1B-diss)-S2B(26;3)	168	154
H_2NNH_3(6;1B-diss)-S2B(26;5)	160[a]	158
H_2NNH_3(6;3B)-S2B(26;3)	177[a]	177
H_2NNH_3(6;3B)-S2B(26;5)	178	183
NH_2(2;1A) + NH_3(26)-S2B(6;HCA)	83[b]	71
NH_2(26) + NH_3(6;HCA)-S2B(2;Cys)	23[b]	14
NH_2(26) + NH_3(6;HCA)-S2B(2;N)	23[b]	24
NH_2(26) + NH_3(2;Cys)-S2B(6;1B)	0[c]	0[c]
NH_2(26) + NH_3(diss)-S2B(6;1B)	29[b]	
NH_2(2;NH_3) + NH_3(diss)-S2B(6;HCA)	58[c]	44[b]

[a] BS-235 state. [b] BS-346 state. [c] BS-156 state.

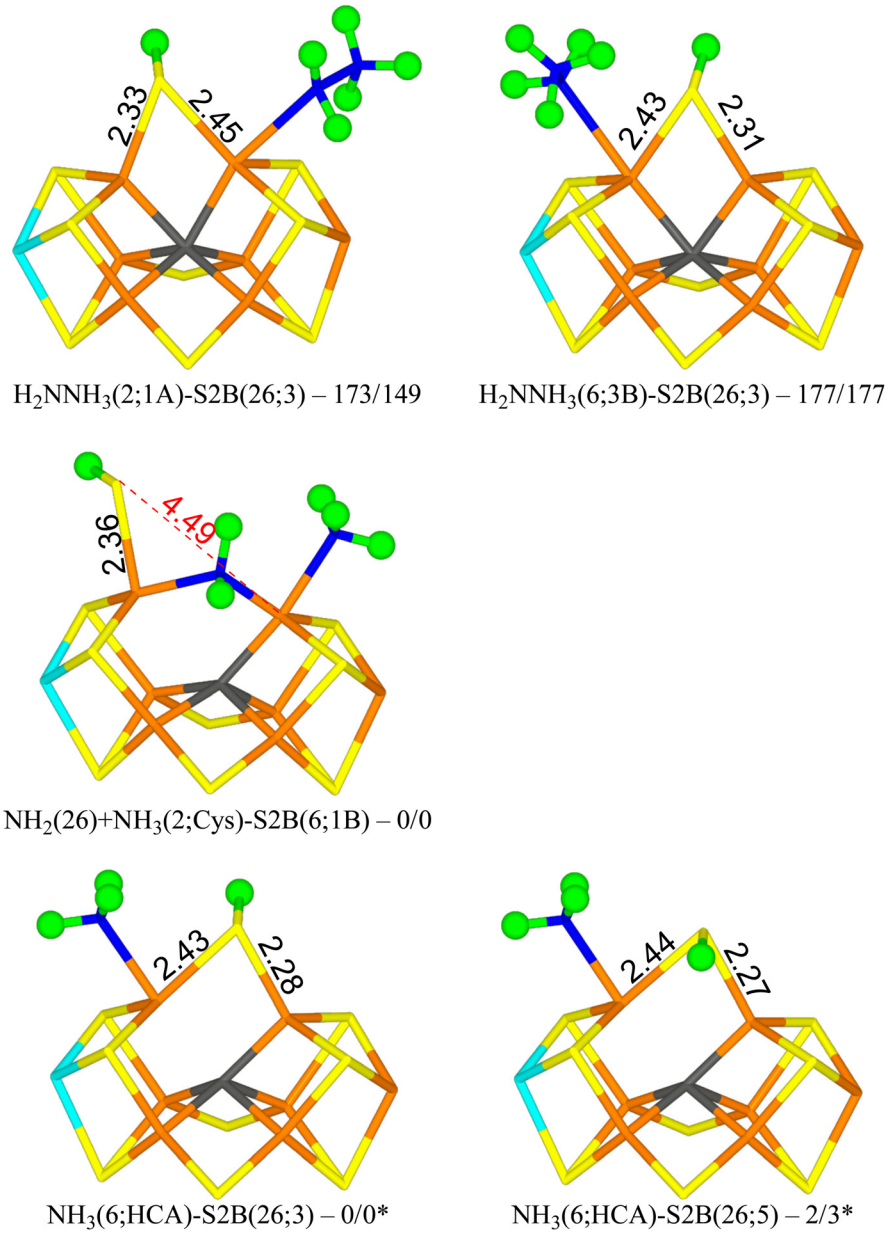

Fig. 5 The E_7 structures with relative energies in kJ mol^{-1} indicated (r^{2}SCAN/TPSSh; * indicates another reference state).

Structures with H_2NNH_3 bound end-on to Fe6 are only 4–5 kJ mol^{-1} less stable with r^{2}SCAN, but 28–34 kJ mol^{-1} less stable with TPSSh. In the best structure (H_2NNH_3(6;3B)-S2B(26;3) in Fig. 5), the non-bonding NH_3 group forms hydrogen bonds to S3B and S2B (2.21 and 2.27 Å). S2B still bridges Fe2 and Fe6, with the proton on the S3A side. If the NH_3 group is moved to the other side, the ligand actually dissociates, giving a structure that is actually 9 kJ mol^{-1} more stable than the best state with r^{2}SCAN but 6 kJ mol^{-1} less stable with TPSSh.

From the H_2NNH_3(2;1A)-S2B(26;3) structure, the N–N bond can easily be cleaved with an activation energy of only 41–50 kJ mol^{-1}. Therefore, we studied several product (NH_2 + NH_3) structures. In the best structure (NH_2(26) + NH_3(2;1A)-S2B (6;1B) in Fig. 5), NH_2 bridges Fe2 and Fe6, whereas NH_3 binds to Fe2, forming a hydrogen bond to S1A (2.67 Å). S2B binds only to Fe6, with the proton pointing towards S1B (3.29 Å). It is most stable in the triplet BS-156 state. This structure is 149–173 kJ mol^{-1} more stable than the best H_2NNH_3 structure. Structures with NH_3 instead binding to Fe6 is only 14–23 kJ mol^{-1} less stable.

NH_3 can dissociate from the FeMo cluster with an activation energy of only 32 kJ mol^{-1}. Therefore, we also studied structures without NH_3 (*i.e.* dissociated and excluded from the calculations). The results are shown in Table 6. The most stable structure has NH_3 bound to Fe6, *i.e.* with a proton abstracted from homocitrate (NH_3(6;HCA)-S2B(26;3) in Fig. 5).

Table 6 Relative energies (kJ mol^{-1}) of the various structures optimised for the E_7 state with NH_3 dissociated. All structures are in the quintet BS-235 state unless otherwise noted

Structure	r^{2}SCAN	TPSSh
NH_2(26)-S2B(2;Cys)	47	35
NH_2(26)-S2B(2;N)	54	42
NH_2(26)-S2B(6;3B)	24	26
NH_2(26)-S2B(6;1B)	26	19
NH_2(2)-S2B(26;3)	78[a]	66
NH_2(2)-S2B(26;5)	75[a]	66
NH_2(2;2A)-S2B(6;3B)	217	
NH_2(6;1B)-S2B(26;3)	77	79
NH_2(6;1B)-S2B(26;5)	76	80
NH_3(6;HCA)-S2B(26;3)	0	0
NH_3(6;HCA)-S2B(26;5)	2	3

[a] BS-147 state.

Table 7 Relative energies (kJ mol^{-1}) of the various structures optimised for the E_8 state. All structures are in the quartet BS-235 state

Structure	r^{2}SCAN	TPSSh
NH_3(2)-S2B(26;3)	0.6	0
NH_3(2)-S2B(26;5)	3	3
NH_3(2)-S2B(6;3B)	26	[a]
NH_3(2)-S2B(6;1B)	16	[a]
NH_3(6)-S2B(26;3)	0.0	5
NH_3(6)-S2B(26;5)	0.1	5
NH_4(diss)-S2B(26;3)	13	22
NH_4(diss)-S2B(26;5)	11	21

[a] Converged to another structure.

One of the protons forms a hydrogen bond to the alcohol O atom of homocitrate (2.23 Å), whereas another is directed towards S2B (2.81 Å). The latter atom bridges Fe2 and Fe6 with the proton on the S3A side. It is most stable in the quintet BS-235 state. A structure with the S2B proton on the other side is 2–3 kJ mol^{-1} less stable (NH_3(6;HCA)-S2B(26;5) in Fig. 5).

Structures with NH_2 bridging Fe2 and Fe6 are at least 19–24 kJ mol^{-1} less stable. They have S2B binding to only one Fe ion, preferably Fe6. Structures with NH_2 binding to either Fe2 or Fe6 (with S2B bridging Fe2 and Fe6) are at least 66–79 or 76–79 kJ mol^{-1} less stable than the NH_3(6;HCA)-S2B(26;3) structure.

E_8 state

Finally, we studied the E_8 state with NH_3 bound to the FeMo cluster. The results are collected in Table 7. Four structures are essentially degenerate (within 5 kJ mol^{-1}). Two have NH_3 bound to Fe6 with one of the protons forming a hydrogen bond to the acetate group of homocitrate (1.87–1.90 Å) and S2B bridging Fe2 and Fe6 with the proton either on the S3A or S5A side (NH_3(6)-S2B(26;3) and NH_3(6)-S2B(26;5) in Fig. 6). The other two have NH_3 bound to Fe2 with the three protons approximately in the directions of SG of Cys-275, S1A and S2A (all distances are 3.0–3.2 Å) and S2B bridging Fe2 and Fe6 with the proton either on the S3A or S5A side (NH_3(2)-S2B(26;3) and NH_3(2)-S2B(26;5) in Fig. 6). Structures with S2B binding only to Fe6 and NH_3 to Fe2 are 16–26 kJ mol^{-1} less stable. Structures with NH_4, where the proton has been abstracted from homocitrate, are 11–13 (r^{2}SCAN) or 21–22 kJ mol^{-1} (TPSSh) less stable and in these NH_4 has dissociated from the cluster (and S2B bridges Fe2 and Fe6). All structures are most stable in the quartet BS-235 state.

Conclusions

We have investigated whether structures with S2B dissociated from either Fe2 or Fe6 may be involved in the second half of the reaction mechanism of nitrogenase. As mentioned in the Introduction, we have previously studied this part of the reaction mechanism assuming either that S2B binds both to Fe2 and Fe6 or that it is fully dissociated from the FeMo cluster.[38,39] However, recent studies have indicated that for the E_2–E_4 states, structures with S2B dissociated from either Fe2 or Fe6 are more stable than structures with a bridging S2B.[22,44,45] Therefore, it is of great interest to know how this finding affects the second half of the reaction mechanism. To make such a half-dissociation possible, we have added one extra proton on S2B, compared to the previous studies. Moreover, we employ two DFT functionals, r^{2}SCAN and TPSSh, which in previous studies have supported and favoured half-dissociation of S2B,[22,44,45] but also giving accurate results for the FeMo cluster of nitrogenase.[58]

Interestingly, we see little advantage of half-dissociation of S2B. For the E_4 and E_5 states, such structures are at least 16–24 and 9–15 kJ mol^{-1} less stable than the best structures with a bridging S2B, respectively. For the E_6 state, structures with a half-dissociated S2B are disfavoured by 47–52 kJ mol^{-1}. However, with NH_3 dissociated, the best E_6 structure has S2B bound only to Fe6, because the NH ligand takes the Fe2–Fe6 bridging position. On the other hand, our results indicate that such structures are not involved in the mechanism. The situation is similar for the E_7 state: With an intact N–N bond, only structures with a bridging S2B ligand is found, whereas after cleavage of N–N bond, NH_2 prefers to bridge between Fe2 and Fe6, forcing S2B to dissociate from Fe2 in the most stable state. However, the substrate may also extract a proton from homocitrate, giving NH_3, which prefers to bind to Fe6 and then S2B goes back to a bridging position. In the E_8 state, NH_3 may bind either to Fe2 or Fe6, but S2B prefers a bridging position by at least 16 kJ mol^{-1}.

Fig. 7 shows our suggested reaction mechanism for nitrogenase with an extra proton on S2B. It contains only a single half-dissociated structure, NH_2(26) + NH_3(2;1A)-S2B(6;1B), and only intermittently during the E_7 state. Therefore, we conclude that half-dissociation of S2B needs to be considered in the reaction mechanism of nitrogenase but seems to be of minor importance during the second half-reaction. The reason for this may be that there are no states with a bridging hydride ion in the second half-reaction.

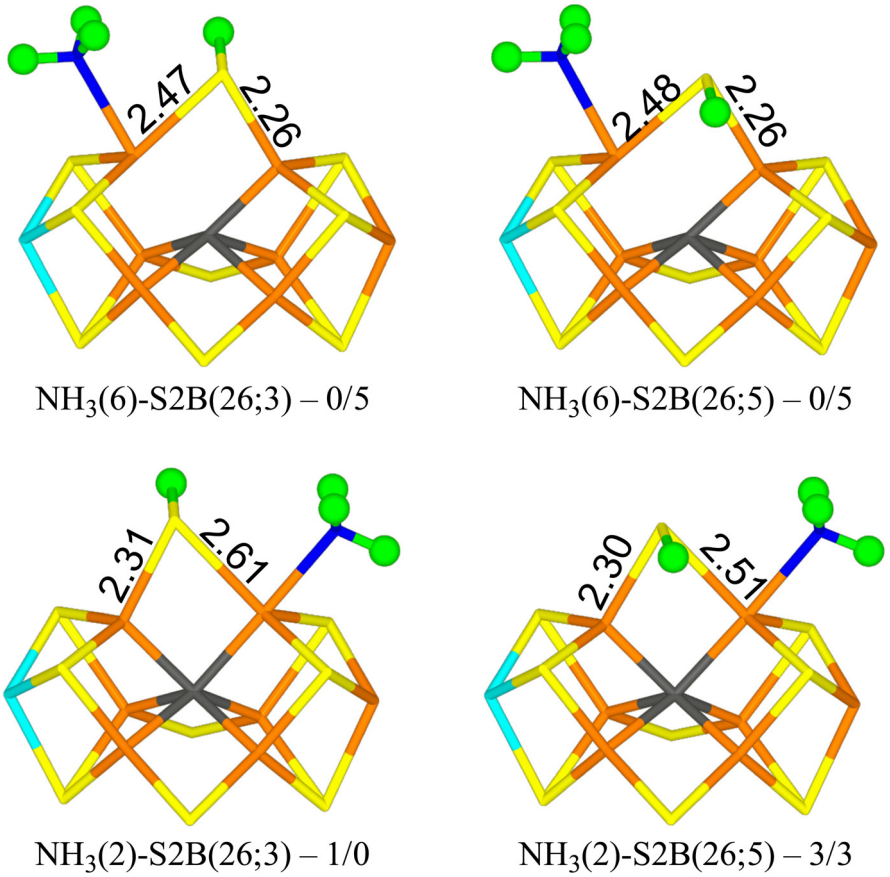

Fig. 6 The best E_8 structures with relative energies in kJ mol^{-1} indicated (r^{2}SCAN/TPSSh).

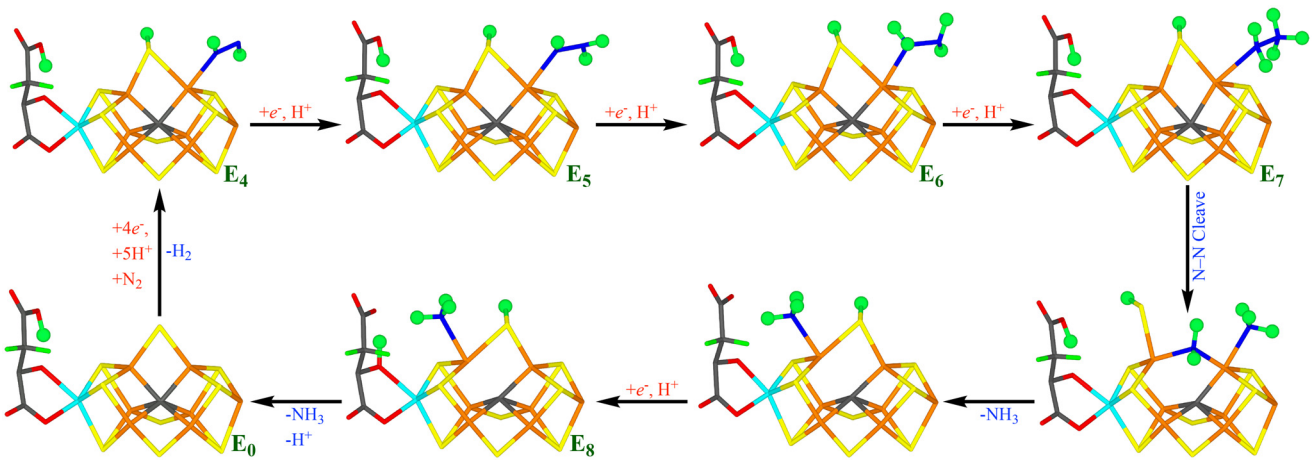

Fig. 7 Suggested reaction mechanism for nitrogenase, assuming that the S2B ligand is protonated.

In this study we have compared the results of two DFT functionals, r^{2}SCAN and TPSSh. The two functionals give similar results for both structures and relative energies. For example, mean absolute deviation of the relative energies calculated with the two methods in Tables 1–7 are 5–10 kJ mol^{-1} and for the most stable structures in Fig. 2–6, the maximum difference in the relative energies is 1–11 kJ mol^{-1}. The only exception is when different BS states are involved; then the difference can increase up to 25 kJ mol^{-1} (for example H_2NNH_3(2;1A)-S2B (26;3) in Fig. 5). Thus, the two functionals give quite similar results although one of them is a meta generalised gradient approximation functional, whereas TPSSh is a hybrid func-

tional with 10% Hartree–Fock exchange. The two functionals were selected because they give accurate structures of nitrogenase models[58] but they also give a stronger preference of half-dissociated structures, *e.g.* compared to pure generalised gradient approximation functionals like TPSS.[45]

Finally, we note that the suggested reaction mechanism is alternating, *i.e.* the protons are added alternating to the two N atoms of the substrate, so that HNNH and H_2NNH_2 are intermediates in the mechanism and that NH_3 does not dissociate until the E_7 state. This is in agreement with our previously suggested mechanism with S2B bridging or dissociated from the cluster.[38,39] On the other hand, the substrate binds preferably to Fe2, which is in contrast to the previously suggested mechanism with a bridging S2B,[39] where the substrate bound preferably to Fe6. The difference seems to come from the protonation of S2B. The protonation state of S2B remains to be settled, but the previous mechanism with unprotonated S2B has the advantage that it employs homocitrate as a proton buffer, which explains why this group is needed for the nitrogenase reaction.[4,85]

Conflicts of interest

There are no conflicts to declare.

Acknowledgements

This investigation has been supported by grants from the Swedish Research Council (project 2022-04978) and from China Scholarship Council. The computations were enabled by resources provided by LUNARC, the Centre for Scientific and Technical Computing at Lund University, and by the National Academic Infrastructure for Supercomputing in Sweden (NAISS) at NSC at Linköping University (Tetralith) and PDC at KTH Royal Institute of Technology (Dardel), partially funded by the Swedish Research Council through grant agreements no. 2022-06725 and 2018-05973.

References

1 B. K. Burgess and D. J. Lowe, *Chem. Rev.*, 1996, **96**, 2983–3012.
2 B. Schmid, H.-J. Chiu, V. Ramakrishnan, J. B. Howard and D. C. Rees, in *Handbook of Metalloproteins*, John Wiley & Sons, Ltd, 2006, pp. 1025–1036, DOI: **10.1002/0470028637.met174**.
3 B. M. Hoffman, D. Lukoyanov, Z.-Y. Yang, D. R. Dean and L. C. Seefeldt, *Chem. Rev.*, 2014, **114**, 4041–4062.
4 L. C. Seefeldt, Z.-Y. Yang, D. A. Lukoyanov, D. F. Harris, D. R. Dean, S. Raugei and B. M. Hoffman, *Chem. Rev.*, 2020, **120**, 5082–5106.
5 T. Spatzal, M. Aksoyoglu, L. Zhang, S. L. A. Andrade, E. Schleicher, S. Weber, D. C. Rees and O. Einsle, *Science*, 2011, **334**, 940–940.
6 J. Kim and D. C. Rees, *Science*, 1992, **257**, 1677–1682.
7 O. Einsle, F. A. Tezcan, S. L. A. Andrade, B. Schmid, M. Yoshida, J. B. Howard and D. C. Rees, *Science*, 2002, **297**, 1696–1696.
8 T. Spatzal, K. A. Perez, O. Einsle, J. B. Howard and D. C. Rees, *Science*, 2014, **345**, 1620–1623.
9 O. Einsle, *J. Biol. Inorg. Chem.*, 2014, **19**, 737–745.
10 A. J. Jasniewski, C. C. Lee, M. W. Ribbe and Y. Hu, *Chem. Rev.*, 2020, **120**, 5107–5157.
11 R. N. F. Thorneley and D. J. Lowe, in *Molybdenum Enzymes*, ed. T. G. Spiro, Wiley, New York, 1985, pp. 221–284.
12 C. Van Stappen, L. Decamps, G. E. Cutsail, R. Bjornsson, J. T. Henthorn, J. A. Birrell and S. DeBeer, *Chem. Rev.*, 2020, **120**, 5005–5081.
13 I. Dance, *ChemBioChem*, 2020, **21**, 1671–1709.
14 Z. Y. Yang, N. Khadka, D. Lukoyanov, B. M. Hoffman, D. R. Dean and L. C. Seefeldt, *Proc. Natl. Acad. Sci. U. S. A.*, 2013, **110**, 16327–16332.
15 D. Lukoyanov, N. Khadka, Z.-Y. Yang, D. R. Dean, L. C. Seefeldt and B. M. Hoffman, *J. Am. Chem. Soc.*, 2016, **138**, 10674–10683.
16 V. Hoeke, L. Tociu, D. A. Case, L. C. Seefeldt, S. Raugei and B. M. Hoffman, *J. Am. Chem. Soc.*, 2019, **141**, 11984–11996.
17 H. Yang, J. Rittle, A. R. Marts, J. C. Peters and B. M. Hoffman, *Inorg. Chem.*, 2018, **57**, 12323–12330.
18 R. Y. Igarashi, M. Laryukhin, P. C. Dos Santos, H.-I. Lee, D. R. Dean, L. C. Seefeldt and B. M. Hoffman, *J. Am. Chem. Soc.*, 2005, **127**, 6231–6241.
19 S. Raugei, L. C. Seefeldt and B. M. Hoffman, *Proc. Natl. Acad. Sci. U. S. A.*, 2018, **115**, 10521–10530.
20 L. Cao and U. Ryde, *J. Chem. Theory Comput.*, 2020, **16**, 1936–1952.
21 A. T. Thorhallsson, B. Benediktsson and R. Bjornsson, *Chem. Sci.*, 2019, **10**, 11110–11124.
22 H. Jiang and U. Ryde, *Dalton Trans.*, 2023, **52**, 9104–9120.
23 P. E. M. Siegbahn, *J. Am. Chem. Soc.*, 2016, **138**, 10485–10495.
24 P. E. M. Siegbahn, *J. Comput. Chem.*, 2018, **39**, 743–747.
25 J. B. Varley, Y. Wang, K. Chan, F. Studt and J. K. Nørskov, *Phys. Chem. Chem. Phys.*, 2015, **17**, 29541–29547.
26 M. Rohde, D. Sippel, C. Trncik, S. L. A. Andrade and O. Einsle, *Biochemistry*, 2018, **57**, 5497–5504.
27 W.-L. Li, Y. Li, J. Li and T. Head-Gordon, *Chem Catal.*, 2023, **3**, 100662.
28 P. E. M. Siegbahn, *Phys. Chem. Chem. Phys.*, 2023, **25**, 23602–23613.
29 J. Chatt, J. R. Dilworth and R. L. Richards, *Chem. Rev.*, 1978, **78**, 589–625.
30 J. Chatt, *Annu. Proc. Phytochem. Soc. Eur.*, 1980, **18**, 1–18.
31 D. V. Yandulov and R. R. Schrock, *Science*, 2003, **301**, 76–78.
32 R. R. Schrock, *Acc. Chem. Res.*, 2005, **38**, 955–962.
33 R. R. Schrock, *Angew. Chem., Int. Ed.*, 2008, **47**, 5512–5522.
34 D. Sippel, M. Rohde, J. Netzer, C. Trncik, J. Gies, K. Grunau, I. Djurdjevic, L. Decamps, S. L. A. Andrade and O. Einsle, *Science*, 2018, **359**, 1484–1489.

35 R. N. F. Thornely, R. R. Eady and D. J. Lowe, *Nature*, 1978, **272**, 557–558.
36 R. N. F. Thorneley and D. J. Lowe, *Biochem. J.*, 1984, **224**, 887–894.
37 D. Lukoyanov, S. A. Dikanov, Z.-Y. Yang, B. M. Barney, R. I. Samoilova, K. V. Narasimhulu, D. R. Dean, L. C. Seefeldt and B. M. Hoffman, *J. Am. Chem. Soc.*, 2011, **133**, 11655–11664.
38 L. Cao and U. Ryde, *J. Catal.*, 2020, **391**, 247–259.
39 H. Jiang and U. Ryde, *Chem. – Eur. J.*, 2022, **28**, e202103933.
40 L. Cao and U. Ryde, *J. Biol. Inorg. Chem.*, 2020, **25**, 521–540.
41 H. Jiang, O. K. G. Svensson, L. Cao and U. Ryde, *Angew. Chem., Int. Ed.*, 2022, **61**, e202208544.
42 P. P. Hallmen and J. Kästner, *Z. Anorg. Allg. Chem.*, 2015, **641**, 118–122.
43 I. Dance, *Dalton Trans.*, 2019, **48**, 1251–1262.
44 A. T. Thorhallsson and R. Bjornsson, *Chem. – Eur. J.*, 2021, **27**, 16788–16800.
45 H. Jiang, O. K. G. Svensson and U. Ryde, *Inorg. Chem.*, 2022, **61**, 18067–18076.
46 L. Cao and U. Ryde, *Phys. Chem. Chem. Phys.*, 2019, **21**, 2480–2488.
47 L. Cao, O. Caldararu and U. Ryde, *J. Phys. Chem. B*, 2017, **121**, 8242–8262.
48 H. Jiang and U. Ryde, *Phys. Chem. Chem. Phys.*, 2024, **26**, 1364–1375.
49 R. Bjornsson, F. Neese and S. DeBeer, *Inorg. Chem.*, 2017, **56**, 1470–1477.
50 B. M. Barney, J. McClead, D. Lukoyanov, M. Laryukhin, T.-c. Yang, D. R. Dean, B. M. Hoffman and L. C. Seefeldt, *Biochemistry*, 2007, **46**, 6784–6794.
51 J. A. Maier, C. Martinez, K. Kasavajhala, L. Wickstrom, K. E. Hauser and C. Simmerling, *J. Chem. Theory Comput.*, 2015, **11**, 3696–3713.
52 W. L. Jorgensen, J. Chandrasekhar, J. D. Madura, R. W. Impey and M. L. Klein, *J. Chem. Phys.*, 1983, **79**, 926–935.
53 L. Hu and U. Ryde, *J. Chem. Theory Comput.*, 2011, **7**, 2452–2463.
54 C. I. Bayly, P. Cieplak, W. D. Cornell and P. A. Kollman, *J. Phys. Chem.*, 1993, **97**, 10269–10280.
55 F. Furche, R. Ahlrichs, C. Hättig, W. Klopper, M. Sierka and F. Weigend, *Wiley Interdiscip. Rev.: Comput. Mol. Sci.*, 2014, **4**, 91–100.
56 J. W. Furness, A. D. Kaplan, J. Ning, J. P. Perdew and J. Sun, *J. Phys. Chem. Lett.*, 2020, **11**, 8208–8215.
57 V. N. Staroverov, G. E. Scuseria, J. Tao and J. P. Perdew, *J. Chem. Phys.*, 2003, **119**, 12129–12137.
58 B. Benediktsson and R. Bjornsson, *J. Chem. Theory Comput.*, 2022, **18**, 1437–1457.
59 A. Schäfer, H. Horn and R. Ahlrichs, *J. Chem. Phys.*, 1992, **97**, 2571–2577.
60 K. Eichkorn, O. Treutler, H. Öhm, M. Häser and R. Ahlrichs, *Chem. Phys. Lett.*, 1995, **240**, 283–289.
61 K. Eichkorn, F. Weigend, O. Treutler and R. Ahlrichs, *Theor. Chem. Acc.*, 1997, **97**, 119–124.
62 E. Caldeweyher, S. Ehlert, A. Hansen, H. Neugebauer, S. Spicher, C. Bannwarth and S. Grimme, *J. Chem. Phys.*, 2019, **150**, 154122–154122.
63 T. Spatzal, J. Schlesier, E.-M. Burger, D. Sippel, L. Zhang, S. L. A. Andrade, D. C. Rees and O. Einsle, *Nat. Commun.*, 2016, **7**, 10902–10902.
64 R. Bjornsson, F. A. Lima, T. Spatzal, T. Weyhermüller, P. Glatzel, E. Bill, O. Einsle, F. Neese and S. DeBeer, *Chem. Sci.*, 2014, **5**, 3096–3103.
65 T. Lovell, J. Li, T. Liu, D. A. Case and L. Noodleman, *J. Am. Chem. Soc.*, 2001, **123**, 12392–12410.
66 L. Cao and U. Ryde, *Int. J. Quantum Chem.*, 2018, **118**, e25627.
67 C. Greco, P. Fantucci, U. Ryde and L. Di Gioia, *Int. J. Quantum Chem.*, 2011, **111**, 3949–3960.
68 R. K. Szilagyi and M. A. Winslow, *J. Comput. Chem.*, 2006, **27**, 1385–1397.
69 U. Ryde, *J. Comput.-Aided Mol. Des.*, 1996, **10**, 153–164.
70 U. Ryde and M. H. M. Olsson, *Int. J. Quantum Chem.*, 2001, **81**, 335–347.
71 N. Reuter, A. Dejaegere, B. Maigret and M. Karplus, *J. Phys. Chem. A*, 2000, **104**, 1720–1735.
72 L. Hu, P. Söderhjelm and U. Ryde, *J. Chem. Theory Comput.*, 2011, **7**, 761–777.
73 L. Cao and U. Ryde, *Front. Chem.*, 2018, **6**, 89–89.
74 I. Mayer, *Chem. Phys. Lett.*, 1983, **97**, 270–274.
75 T. Lu and F. Chen, *J. Comput. Chem.*, 2012, **33**, 580–592.
76 I. Dance, *J. Am. Chem. Soc.*, 2005, **127**, 10925–10942.
77 I. Dance, *Dalton Trans.*, 2012, **41**, 7647–7659.
78 I. Dance, *Inorg. Chem.*, 2013, **52**, 13068–13077.
79 I. Dance, *Dalton Trans.*, 2015, **44**, 18167–18186.
80 I. Dance, *J. Inorg. Biochem.*, 2017, **169**, 32–43.
81 I. Dance, *Biochemistry*, 2006, **45**, 6328–6340.
82 P. E. M. Siegbahn, *J. Phys. Chem. B*, 2023, **127**, 2156–2159.
83 L. C. Seefeldt, I. G. Dance and D. R. Dean, *Biochemistry*, 2004, **43**, 1401–1409.
84 S. J. George, B. M. Barney, D. Mitra, R. Y. Igarashi, Y. Guo, D. R. Dean, S. P. Cramer and L. C. Seefeldt, *J. Inorg. Biochem.*, 2012, **112**, 85–92.
85 J. Imperial, T. R. Hoover, M. S. Madden, P. W. Ludden and V. K. Shah, *Biochemistry*, 1989, **28**, 7796–7799.